4MPo1D-01

Resistance and Voltage–Current Characteristics of REBCO Superconducting Joint

Yasuaki Takeda, Gen Nishijima, and Hitoshi Kitaguchi

***Abstract*— We discuss resistance and voltage–current characteristics of a $REBa_2Cu_3O_y$ (REBCO, RE = rare earth) intermediate grown superconducting (iGS) joint. These characteristics are evaluated based on the current decay measurements for a REBCO closed loop. The temperature and magnetic field dependencies of the *n* value for the iGS joint, assessed using an empirical power-law model, are similar to those observed for REBCO tapes. The percolation model describes the voltage–current characteristics of the iGS joint more accurately. Using the critical current and *n* values at 10^{-8} V, we can approximately estimate the upper limit of the current for a low target resistance.**

***Index Terms*—2G HTS conductors, coated conductors, resistance measurement, critical current**

I. Introduction

Superconducting joints are essential for a superconducting magnet operated in the persistent mode [1][2]. Recently, significant progress has been made in developing superconducting joints between high-temperature superconductors (HTSs) [3]–[12]. The persistent mode operation of closed HTS coils and loops with HTS joints has been successfully demonstrated.

For REBCO HTS tapes, Ohki et al. developed an intermediate grown superconducting (iGS) joint [5]. In this design, REBCO thin films of the joined tapes are connected via an epitaxially grown REBCO intermediate layer. The iGS joints exhibit high critical current and low resistance. A nuclear magnetic resonance (NMR) magnet was successfully operated in the persistent mode using the REBCO insert coil closed with the iGS joints [13]. The iGS joint is considered the most promising solution for achieving a superconducting joint between REBCO tapes.

We have evaluated joint critical current (I_{cj}) and joint resistance (R_j) characteristics for both REBCO and $(Bi,Pb)_2Sr_2Ca_2Cu_3O_y$ (Bi-2223) superconducting joints [14]–[21]. The temperature, magnetic field, and field angular dependencies of I_{cj} have been evaluated. The I_{cj} characteristics are similar to those of the HTS tapes. We have also evaluated the dependence of R_j not only on the temperature, field, and field angle but also on the time and current. The R_j value is primarily determined by the load factor, defined as the ratio of the current flowing in the joint to I_{cj}. The time dependence of R_j can be explained by considering flux creep within the joint. Our studies have suggested that the I_{cj} and R_j characteristics can be understood using the conventional models for HTS tapes.

For an HTS magnet containing superconducting joints operated in the persistent mode, R_j at the operating current must be sufficiently low. Evaluating resistance below 10^{-12} Ω using common transport measurement methods is challenging. Low R_j values are usually evaluated by the current decay measurements [22][23], but the measurements are time-consuming. The R_j evaluation system we have developed enables more efficient measurements than before [24]. However, it still takes a long time to evaluate R_j under various measurement conditions, such as currents, magnetic fields, and temperatures. It would be useful if such a low R_j, that is, a low voltage at a given current, could be estimated from the voltage–current characteristics in the voltage range that can be evaluated using common methods.

In this study, we evaluate and discuss R_j and voltage–current characteristics of the REBCO iGS joint. We measure herein the decay of the current flowing in a REBCO closed-loop sample with the iGS joint. Assuming that the critical current of the tape outside the joint is sufficiently higher than I_{cj}, the joint characteristics can be evaluated from the current decay data. We propose a method for estimating the current that can flow in the joint while maintaining a certain R_j. This method extrapolates the I_{cj} and *n* values at 10^{-8} V to the low-voltage range using an empirical power-law model. Additionally, we discuss the voltage–current characteristics using the percolation model.

II. Experimental

We conducted current decay measurements for a single-turn REBCO closed-loop sample containing the iGS joint. The diameter of the loop was 10 cm. The self-inductance (L) of the sample was 0.47 μH. For the current decay measurements, we utilized the joint resistance evaluation system previously developed [16][24]. In this setup, a loop current (I_{loop}) was induced in the sample through magnetic induction using a copper coil positioned at the center of the loop. The decay of I_{loop}, representing its time (t) dependence, was recorded at a sampling rate of 1 Hz. Measurements were performed at temperatures (T) ranging from 30 to 85 K and magnetic fields

Submitted for review September 25, 2024.

This work was supported by JST-Mirai Program Grant Number JPMJMI17A2 and JSPS KAKENHI Grant Number JP22K14482, Japan. *(Corresponding author: Yasuaki Takeda.)*

Yasuaki Takeda, Gen Nishijima, and Hitoshi Kitaguchi are with National Institute for Materials Science (NIMS), Tsukuba, Ibaraki 305-0047, Japan (e-mail: TAKEDA.Yasuaki@nims.go.jp).

Color versions of one or more of the figures in this article are available online at http://ieeexplore.ieee.org

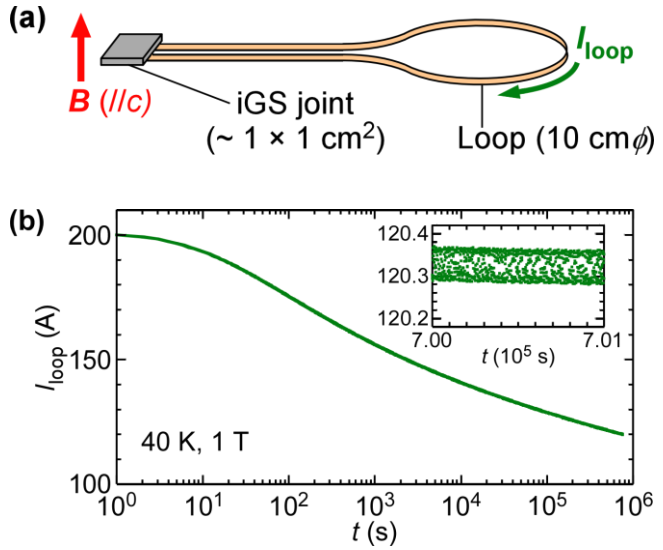

Fig. 1. (a) Schematic of single-turn REBCO closed-loop sample containing the iGS joint. Magnetic field (B) parallel to the c-axis is applied to the joint. (b) Time dependence of I_{loop} at 40 K and 1 T. The inset shows a magnified view at 7.00–7.01 × 10^5 s. As time progresses, ΔI_{loop} decreases, leading to a lower signal-to-noise ratio.

(B) between 0.1 and 1 T, with the field aligned parallel to the c-axis of the REBCO iGS joint, as shown in Fig. 1(a).

Fig. 1(b) illustrates the time dependence of the I_{loop} at 40 K and 1 T, which is the typical result of the current decay measurements. We introduced the initial I_{loop} higher than joint critical current (I_{cj}). This is because the decay of I_{loop} is clearly observed, as shown in Fig. 1(b). To evaluate joint resistance (R_j), data points of the time dependence of I_{loop} were fitted to the following equation using the least-squares method:

$$I_{loop}(t) = I_{loop}(0)\exp\left(-\frac{R_j}{L}t\right). \quad (1)$$

Here, the initial I_{loop} was introduced at t = 0. Our previous study demonstrated that R_j is time-dependent [18]. Since I_{loop} is also time-dependent, we determined the R_j value corresponding to each I_{loop} by fitting the I_{loop}–t data to (1) across various time intervals.

To evaluate I_{cj}, the voltage across the joint (V_j) was calculated from the time dependence of I_{loop} using the following equation:

$$V_j = -L\frac{\Delta I_{loop}}{\Delta t}. \quad (2)$$

The I_{loop} dependence of V_j was smoothed using a 25-point moving average. From the smoothed V_j–I_{loop} curve within the voltage range of 0.5–2 × 10^{-8} V, we determined I_{cj} from I_{loop} based on the voltage criterion (V_c) of 10^{-8} V [19]. For this sample, the I_{cj} value at 77 K in the self-field was evaluated to be 80 A.

As shown in the inset of Fig. 1(b), a magnified view of I_{loop}–t at 7.00–7.01 × 10^5 s, ΔI_{loop} decreases as time progresses,

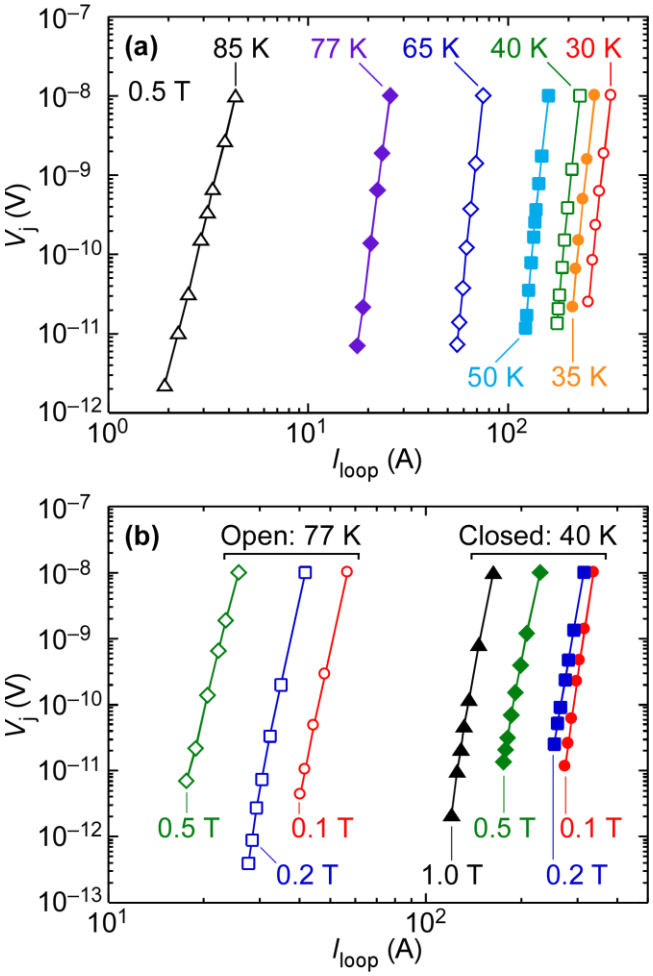

Fig. 2. V_j–I_{loop} curves obtained from the current decay measurements (a) in 0.5 T and at temperatures ranging from 30 to 85 K, and (b) in magnetic fields ranging from 0.1 to 1 T and at 40 and 77 K. All curves exhibit upward concavity or a power-law dependence. An empirical power-law model is applicable to the low-voltage range.

leading to a lower signal-to-noise ratio. This reduced signal-to-noise ratio made it challenging to evaluate V_j values below 10^{-8} V using (2). To address this, we used the equation V_j = R_jI_{loop} along with the R_j value at each I_{loop} obtained from (1) to derive the V_j–I_{loop} curves at voltages lower than 10^{-8} V.

III. Results and Discussion

A. *Voltage–current characteristics*

Fig. 2 shows the V_j–I_{loop} curves obtained from the current decay measurements at temperatures ranging from 30 to 85 K and magnetic fields between 0.1 and 1 T. All curves exhibit upward concavity or a power-law dependence, suggesting that the vortex glass-liquid transition [25] was not observed under the given measurement conditions ($T \le T_{GL}$ and $B \le B_{GL}$).

Considering that the slope of the V_j–I_{loop} curves is almost constant at the low-voltage range, we applied the following empirical power-law model to the curves:

$$V_j = V_c \left(\frac{I_{loop}}{I_{cj}}\right)^n. \quad (3)$$

We obtained n values using (3) by fitting the V_j–I_{loop} curves at the voltage range of $0.2–2 \times 10^{-10}$ V. Fig. 3 presents the obtained n values over the temperature range of 30–85 K and field range of 0.1–1 T. We also show the n values in the range of $0.5–2 \times 10^{-8}$ V calculated from the smoothed V_j–I_{loop} curve to determine I_{cj} with $V_c = 10^{-8}$ V. With a decrease in the voltage from 10^{-8} to 10^{-10} V, the n values were increased. The maximum increase in the n value was 8.4.

In the temperature dependence plot of n values at 0.5 T, shown in Fig. 3(a), a plateau exists between 30 and 65 K for n values obtained within the range of $0.5–2 \times 10^{-8}$ V. Additionally, the variation of the n value obtained at $0.2–2 \times 10^{-10}$ V appears to be small in the range of 30–65 K. In contrast, the n values were decreased from 65 to 85 K. Similar temperature dependence is reported in the transport measurements for REBCO tapes, where the electric field criterion is 10^{-6} V cm^{-1} [26][27]. As shown in Fig. 3(b), n values at 40 and 77 K decreased as the fields increased from 0.1 to 0.5 T. At 40 K, the n value remained nearly constant from 0.5 to 1 T. Similar field dependence is also reported for the transport measurements of a REBCO tape [28] and iGS joints [13]. These findings suggest that the field and temperature dependencies of the n value at the low-voltage criterion for the REBCO iGS joint are similar to those for REBCO tapes.

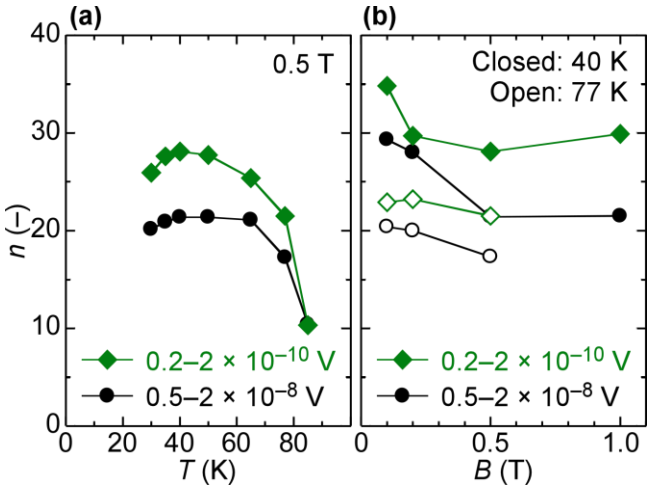

Fig. 3. Dependencies of the n values on (a) temperature at 0.5 T and (b) magnetic field at 40 and 77 K. The temperature and field dependencies of the n values are similar to those for REBCO tapes evaluated based on transport measurements.

B. Estimation of load factor for low-target resistance using the critical current and n values

As shown in Fig. 3, the increase in the n value was not significant at decreasing voltages. This implies that R_j values in the range of 10^{-12}–10^{-13} Ω can be approximately estimated from the I_{cj} and n values at 10^{-8} V. From the power-law model (3) and the equation $V_j = R_j I_{loop}$, we obtain the following equation,

$$R_j = \frac{V_c}{I_{cj}} F^{n-1}, \quad (4)$$

where $F = I_{loop}/I_{cj}$ is the load factor. Given an F value, the corresponding R_j values can be calculated using the I_{cj} and n values at 10^{-8} V. Conversely, given a target R_j, the upper limit of F can be calculated using the following equation obtained from (4),

$$F = \left(\frac{R_j I_{cj}}{V_c}\right)^{\frac{1}{n-1}}. \quad (5)$$

Fig. 4(a) shows the temperature dependence of the I_{cj} and n values at 10^{-8} V and 0.5 T. Using these I_{cj} and n values, the temperature dependence of R_j is calculated for F values in the range of 0.4–0.9, as shown in Fig. 4(b). As suggested in (4), R_j increases with increasing F values.

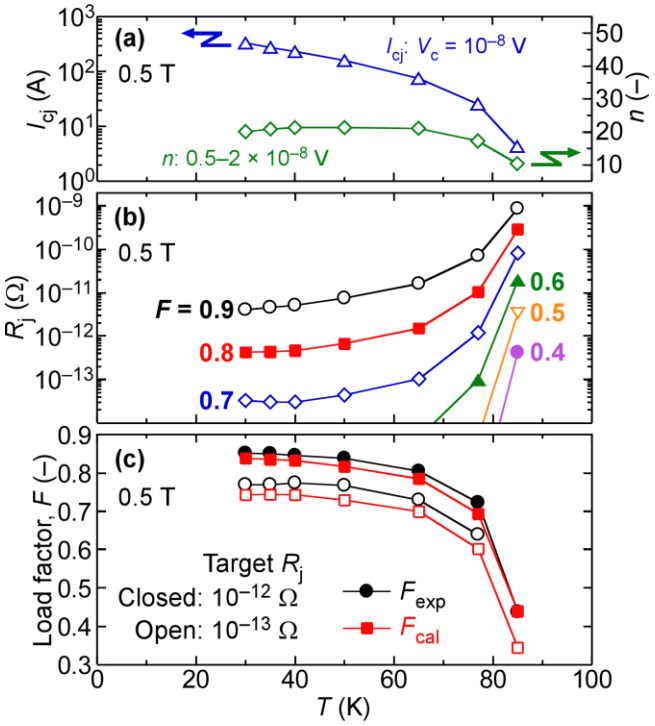

Fig. 4. (a) Temperature dependence of the I_{cj} and n values at 0.5 T and 10^{-8} V. (b) Temperature dependence of R_j calculated using the I_{cj} and n values shown in (a) with F values in the range of 0.4–0.9 using (4). R_j increases at increasing temperatures; this is due to the decrease in the I_{cj} and n values. (c) Temperature dependence of F at 0.5 T for the target R_j values of 10^{-12} and 10^{-13} Ω. The F_{cal} values show good agreement with the F_{exp} values.

Fig. 4(b) shows that as the temperature increases, R_j also increases. From 30 to 65 K, I_{cj} decreases exponentially while the n value remains almost constant, as shown in Fig. 4(a).

This suggests that the slight increase in R_j at higher temperatures in the range of 30–65 K is due to the exponential decrease in I_{cj}. In contrast, a larger increase in R_j is observed from 65 to 85 K. This is due to the considerable decrease in both the I_{cj} and n values at increasing temperatures, as shown in Fig. 4(a).

Fig. 4(c) shows the temperature dependence of the F values at 0.5 T for the target R_j values of 10^{-12} and 10^{-13} Ω. The experimentally obtained F (F_{exp}) values and the calculated F (F_{cal}) values using (5) are shown. The F values decrease slightly with increasing temperatures up to 65 K and drop rapidly at higher temperatures. The rapid decrease in the F values is due to the significant decrease in both the I_{cj} and n values. This corresponds to the earlier discussion of the increase in R_j in the previous paragraph.

The F_{cal} values show good agreement with the F_{exp} values. The maximum differences between these F values are 2.9% and 3.7% for the target R_j values of 10^{-12} and 10^{-13} Ω, respectively. This indicates that the upper limit of F for target R_j in the range of 10^{-12}–10^{-13} Ω can be approximately estimated using the I_{cj} and n values at 10^{-8} V.

We also examined the magnetic field dependence of R_j and F. Fig. 5(a) shows the field dependence of the I_{cj} and n values at 10^{-8} V at 40 and 77 K. Using these values, R_j is calculated as shown in Fig. 5(b). R_j increases with increasing field, primarily due to the decrease in the I_{cj} and n values.

Figs. 5(c) and 5(d) illustrate the field dependence of F_{exp} and F_{cal} for the target R_j values of 10^{-12} and 10^{-13} Ω, respectively, at 40 and 77 K. The decrease in F values at increasing fields is attributed to the reduction in both I_{cj} and n values. The F_{cal} values are consistent with the F_{exp} values, with maximum differences of 2.9% and 4.5% for target R_j values of 10^{-12} and 10^{-13} Ω, respectively. These findings demonstrate that the upper limit of F for target R_j values in the range of 10^{-12}–10^{-13} Ω can be approximately estimated.

From Figs. 4(c), 5(c), and 5(d), the difference between F_{exp} and F_{cal} for a target R_j value of 10^{-13} Ω is larger than that for 10^{-12} Ω. As most of the V_j–I_{loop} curves exhibit upward concavity, the difference increases at lower R_j values. In the next section, we discuss the relationship between the V_j–I_{loop} characteristics and the validity of the estimation of the F values for a low target R_j.

C. Application of the percolation model to voltage–current characteristics

Most of the V_j–I_{loop} curves shown in Fig. 2 exhibit upward concavity and are steeper in the low-voltage range. This behavior corresponds to the increase in the n values at decreasing voltages, as shown in Fig. 3. The percolation model [29][30], rather than the power-law model, may be more appropriate for describing the V_j–I_{loop} curves. The following equation, which was modified from an equation in [30], was used:

$$V_j = \frac{A}{m} I_{loop}{}^m \left(1 - \frac{I_{cjm}}{I_{loop}}\right)^m, \quad (6)$$

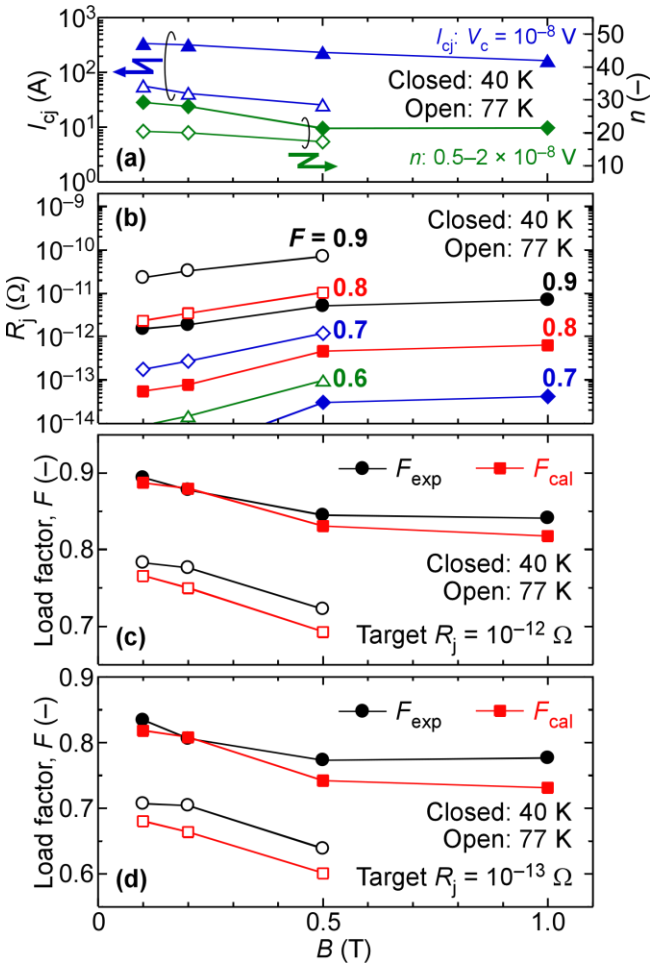

Fig. 5. (a) Magnetic field dependence of the I_{cj} and n values at 10^{-8} V, at 40 and 77 K. (b) Field dependence of R_j calculated using the I_{cj} and n values shown in (a) with F values in the range of 0.6–0.9 using (4). R_j increases at increasing fields, which is due to the decrease in I_{cj} and n values. (c) Field dependence of F at 40 and 77 K for target R_j of 10^{-12} Ω and (d) 10^{-13} Ω. The F_{cal} values are consistent with the F_{exp} values.

where A and m are the fitting parameters, and I_{cjm} is the minimum I_{cj} of the distribution of critical current.

The percolation model describes the relationship between the electric field (E) and current density (J), effectively capturing an upward concave log E–log J curve over a wide current density range of approximately 10^2–10^6 A cm^{-2} [29]–[31]. Determining the cross-sectional area (S) of the current flowing in the iGS joint is challenging because the current path and effective joint area are not fully understood. However, S is less than the tape's area in the joint, estimated to be within the range of 10^{-1}–10^0 cm^2. Assuming the effective joint area is 10% of the apparent joint area, S will be in the range of 10^{-2}–10^{-1} cm^2. For the iGS joint, since S is estimated to be within 10^{-2}–10^0 cm^2, a current range of 10^2–10^3 A corresponds to a current density range of 10^2–10^5 A cm^{-2}. Thus, the percolation model is expected to describe the V_j–I_{loop} behavior at 40 K in the current range of 1–4 × 10^2 A, as shown in Fig. 2(b).

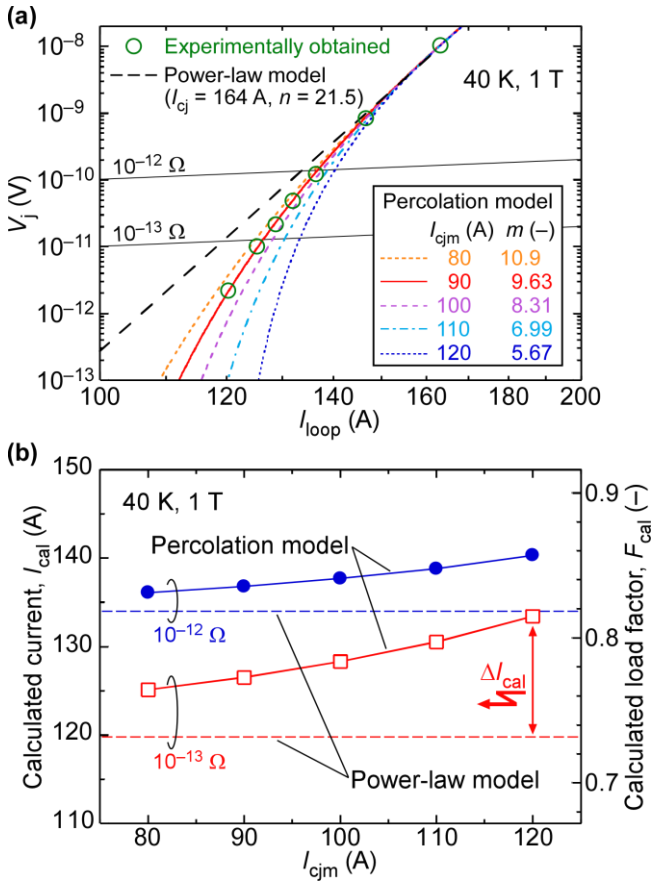

Fig. 6. (a) V_j–I_{loop} plots at 40 K and 1 T with the experimentally obtained values displayed in Fig. 2(b). The straight dashed line corresponds to the power-law model using the I_{cj} and n values at 10^{-8} V. The curves obtained using (6) with I_{cjm} values in the range of 80–120 A are shown. (b) I_{cjm} dependence of I_{cal} and F_{cal} for the target R_j values of 10^{-12} and 10^{-13} Ω. The dashed lines represent the I_{cal} and F_{cal} values obtained using the power-law model. As the I_{cjm} increases, the difference between the I_{cal} values obtained using the percolation and power-law models (ΔI_{cal}) increases as well.

Fig. 6(a) shows the V_j–I_{loop} plots at 40 K and 1 T with the experimentally obtained values displayed in Fig. 2(b). The straight dashed line corresponds to the power-law model (3) using the I_{cj} and n values at 10^{-8} V. The curves obtained using (6) with I_{cjm} values in the range of 80–120 A are also shown. The A and m values are determined from the I_{cj} and n values at 10^{-8} V. Note that the I_{cjm} value of 120 A is high, as the calculated curve yields an I_{loop} value of 126 A at 10^{-13} V, which is comparable to the I_{cjm}.

As the I_{cjm} increases, the V_j–I_{loop} curve obtained using (6) becomes steeper. The experimental data are well-fitted by the calculated curve with I_{cjm} = 90 A. This indicates that the V_j–I_{loop} behavior of the iGS joint can be described by the percolation model.

In the previous section, the upper limit of F_{cal} was obtained for a target R_j. This means that the upper limit of the calculated current I_{cal} (F_{cal} = I_{cal}/I_{cj}) was approximately estimated for a target R_j. The resistance lines of 10^{-12} and 10^{-13} Ω are also shown in Fig. 6(a). The I_{loop} value at the intersection of the resistance line and the dashed line agrees with I_{cal} for the target R_j. The intersection of the resistance line and the calculated curve when I_{cjm} = 90 A corresponds to the experimental I_{loop} values for the target R_j, as this curve describes the experimental V_j–I_{loop}. If the experimentally obtained V_j–I_{loop} curve yields higher I_{cjm}, the I_{loop} value at the intersection will increase.

Fig. 6(b) shows the I_{cjm} dependence of I_{cal} and F_{cal} for the target R_j values of 10^{-12} and 10^{-13} Ω, calculated using the percolation model (6). The dashed lines represent I_{cal} and F_{cal} derived from the power-law model.

We discuss the difference between the I_{cal} values obtained using the percolation and power-law models, denoted as ΔI_{cal}. Fig. 6(b) demonstrates that larger ΔI_{cal} values are observed for 10^{-13} Ω compared to those for 10^{-12} Ω. At I_{cjm} = 90 A, ΔI_{cal} is only 6.8 A for 10^{-13} Ω, corresponding to a difference in F_{cal} of 4.5%. Considering that the curve with I_{cjm} = 90 A describes the experimental V_j–I_{loop} shown in Fig. 6(a), the upper limit of the current for the target R_j value of 10^{-13} Ω could be approximately estimated using the power-law model.

Fig. 6(b) also shows that as the I_{cjm} increases, ΔI_{cal} increases as well. At I_{cjm} = 120 A, ΔI_{cal} is 14 A for 10^{-13} Ω, which corresponds to a difference in F_{cal} of 8.7%. This suggests that at increasing I_{cjm}, the upper limit of the current for a low target R_j value is estimated less accurately using the power-law model.

D. Discussion

From the discussion of ΔI_{cal} in the previous section, the proposed method to estimate the upper limit of the current flowing in the iGS joint while maintaining R_j values in the range of 10^{-12}–10^{-13} Ω leads to the following conclusions:

- When I_{cjm} is not high, the upper limit of the current can be approximately estimated using the I_{cj} and n values at 10^{-8} V, as demonstrated in this study. The difference between practical current and I_{cal} values required to maintain a target R_j will be small, corresponding to F values of less than 5%.
- When I_{cjm} is high and comparable to the current at 10^{-13} V, the difference between the practical current and I_{cal} for a target R_j will be large and will correspond to an F value of approximately 10% for R_j = 10^{-13} Ω. This implies that the upper limit of the current is estimated less accurately. Note that since I_{cal} is underestimated, R_j values lower than the target value will be achieved at the I_{cal}.

In previous studies, we clarified that the microstructure of the intermediate layer of the Bi-2223 superconducting joint strongly affects the I_{cj} characteristics [20][32]. Regarding the iGS joint, the improvement of the microstructure is expected to increase the critical current and enhance the voltage–current characteristics at higher I_{cjm} values. Previous studies showed the misorientations and secondary phases in the intermediate layer of the iGS joint [5][33]. The microstructure may be improved by controlling the chemical composition and

constituent phase of the intermediate layer or optimizing the heat-treatment condition.

Evaluating the I_{cj} and n values at 10^{-8} V through common transport measurements is challenging. The voltage criterion of 10^{-6}–10^{-7} V is typically used for transport measurements [2]. Estimating low R_j values using the I_{cj} and n values within this voltage range can be problematic due to the influence of current sharing caused by the inhomogeneous current distribution in the joint [18].

Magnetic relaxation measurements may be applicable for evaluating the I_{cj} and n values at 10^{-8} V. This is because E approximately equal to 10^{-8} V cm^{-1} is observed during magnetic relaxation of a REBCO tape within a few seconds [34]. A technical problem may be the relatively large size of the iGS joint, as shown in Fig. 1(a). It should also be determined whether these measurements can be conducted while the joints are connected to the coil. If magnetic relaxation measurements can be applied to iGS joints implemented in a REBCO coil, the determination of whether the coil joints show sufficiently low R_j values at the operating current may be allowed by evaluating the I_{cj} and n values at 10^{-8} V. We plan to evaluate the I_{cj} and n values of an iGS joint using magnetic relaxation measurements.

We evaluated the joint characteristics assuming that the critical current of the tape outside the joint is sufficiently higher than I_{cj}. However, this assumption is not always correct. It has been reported that the critical current of a REBCO tape can be degraded by applying temperatures and pressures similar to those used to fabricate a superconducting joint [35]. We should consider evaluating the distribution of the critical current throughout the closed-loop sample, including the iGS joint.

IV. Conclusion

We evaluated the resistance and voltage–current characteristics of the iGS joint based on the current decay measurements for a single-turn REBCO closed loop. The temperature and magnetic field dependencies of the n value for the iGS joint were similar to those observed for REBCO tapes. The percolation model was found to describe the voltage–current characteristics of the iGS joint more accurately than the power-law model. We approximately estimated the upper limit of the current that can flow through the joint to maintain a low R_j value using critical current and n values at 10^{-8} V. This estimation method is applicable when the minimum critical current of the joint is not high. Although evaluating the critical current and n values at 10^{-8} V using common transport measurements is challenging, magnetic relaxation measurements may be applicable for iGS joints. This approach may help determine whether iGS joints implemented in a REBCO coil achieve the low resistance required at the operating current.

Acknowledgment

The authors would like to thank Dr. Mamoru Hamada of Japan Superconductor Technology, Inc., and Dr. Kotaro Ohki of Sumitomo Electric Industries, Ltd., for providing the samples.

References

[1] G. D. Brittles, T. Mousavi, C.R.M. Grovenor, C. Aksoy, and S.C. Speller, “Persistent current joints between technological superconductors,” *Supercond. Sci. Technol.*, vol. 28, no. 9, Aug. 2015, Art. no. 093001.

[2] Y. Takeda, H. Maeda, K. Ohki, and Y. Yanagisawa, “Review of the temporal stability of the magnetic field for ultra-high field superconducting magnets with a particular focus on superconducting joints between HTS conductors,” *Supercond. Sci. Technol.*, vol. 35, no. 4, Apr. 2022, Art. no. 043002.

[3] Y. Park, M. Lee, H. Ann, Y.H. Choi, and H. Lee, “A superconducting joint for $GdBa_2Cu_3O_{7-\delta}$-coated conductors,” *NPG Asia Mater*, vol. 6, May 2014, Art. no. e98.

[4] X. Jin, Y. Yanagisawa, H. Maeda, and Y. Takano, “Development of a superconducting joint between a $GdBa_2Cu_3O_{7-\delta}$-coated conductor and $YBa_2Cu_3O_{7-\delta}$ bulk: towards a superconducting joint between RE (Rare Earth) $Ba_2Cu_3O_{7-\delta}$-coated conductors,” *Supercond. Sci. Technol.*, vol. 28, no. 7, Jun. 2015, Art. no. 075010.

[5] K. Ohki *et al*., “Fabrication, microstructure and persistent current measurement of an intermediate grown superconducting (iGS) joint between REBCO-coated conductors,” *Supercond. Sci. Technol.*, vol. 30, no. 11, Oct. 2017, Art. no. 115017.

[6] P. Chen *et al*., “Development of a persistent superconducting joint between Bi-2212/Ag-alloy multifilamentary round wires,” *Supercond. Sci. Technol.*, vol. 30, no. 2, 2017, Art. no. 025020.

[7] S. Mukoyama *et al*., “Superconducting joint of REBCO wires for MRI magnet,” *J. Phys.: Conf. Ser.* vol. 1054, 2018, Art. no. 012038.

[8] Y. Takeda *et al*., “High I_c superconducting joint between Bi2223 tapes,” *Appl. Phys. Express*, vol. 12, no. 2, Feb. 2019, Art. no. 023003.

[9] X. Jin *et al*., “Superconducting joint between multi-filamentary $Bi_2Sr_2Ca_2Cu_3O_{10+\delta}$ tapes based on incongruent melting for NMR and MRI applications,” *Supercond. Sci. Technol.*, vol. 32, no. 3, Feb. 2019, Art. no. 035011.

[10] T. Mousavi, S. Santra, Z. Melhem, S. Speller, and C. Grovenor, “Superconducting Joint Structures For Bi-2212 Wires Using a Powder-in-Tube Technique,” *IEEE Trans. Appl. Supercond.*, vol. 31, no. 5, Aug. 2021, Art. no. 6400504.

[11] D. Huang *et al*., “An efficient approach for superconducting joint of YBCO coated conductors,” *Supercond. Sci. Technol.*, vol. 35, no. 7, May 2022, Art. no. 075004.

[12] P. Zagura *et al*., “Development of persistent joints for superconducting Bi-2212 coils,” *Supercond. Sci. Technol.*, vol. 37, no. 5, Apr. 2024, Art. no. 055003.

[13] Y. Yanagisawa *et al*., “Development of a persistent-mode NMR magnet with superconducting joints between high-temperature superconductors,” *Supercond. Sci. Technol.*, vol. 34, no. 11, Sep. 2021, Art. no. 115006.

[14] G. Nishijima *et al*., “Transport Property of REBCO Superconducting Joints in Magnetic Fields at Various Temperatures,” *IEEE Trans. Appl. Supercond.*, vol. 29, no. 5, Aug. 2019, Art. no. 6602105.

[15] Y. Takeda *et al*., “Critical current improvement and resistance evaluation of superconducting joint between Bi2223 tapes,” *Supercond. Sci. Technol.*, vol. 35, no. 2, Feb. 2022, Art. no. 02LT02.

[16] K. Kobayashi *et al*., “In-Field Evaluation of REBCO Superconducting Joint,” *IEEE Trans. Appl. Supercond.*, vol. 32, no. 6, Sep. 2022, Art. no. 6601404.

[17] Y. Takeda, G. Nishijima, K. Kobayashi, and H. Kitaguchi, “Fabrication of Bi-2223 Superconducting Joint by Hot-Pressing Process,” *IEEE Trans. Appl. Supercond.*, vol. 33, no. 5, Aug. 2023, Art. no. 6400207.

[18] Y. Takeda, G. Nishijima, and Y. Tsuchiya, “Interpretation of time-dependent current and resistance of HTS closed loop with superconducting joint considering flux creep,” *Appl. Phys. Express*, vol. 16, no. 9, Sep. 2023, Art. no. 093002.

[19] Y. Takeda, G. Nishijima, U. Nakai, T. Motoki, J. Shimoyama, and H. Kitaguchi, “Angular dependence of resistance and critical current of a

Bi-2223 superconducting joint," *Supercond. Sci. Technol.*, vol. 36, no. 12, Oct 2023, Art. no. 125010.

[20] Y. Takeda, G. Nishijima, U. Nakai, T. Motoki, J. Shimoyama, and H. Kitaguchi, "Angular Dependence of Critical Current and Grain Alignment in Bi-2223 Superconducting Joint," *IEEE Trans. Appl. Supercond.*, vol. 34, no. 5, Aug. 2024, Art. no. 6400305.

[21] Y. Takeda, G. Nishijima, T. Motoki, J. Shimoyama, and H. Kitaguchi *et al*., "Temperature, field, and field angular dependence of critical current of REBCO intermediate grown superconducting joint," to be submitted.

[22] M. J. Leupold and Y. Iwasa, "Superconducting joint between multifilamentary wires 1. Joint-making and joint results," *Cryogenics*, vol. 16, no. 4, pp. 215–216, Apr. 1976.

[23] Y. Iwasa, "Superconducting joint between multifilamentary wires 2. Joint evaluation technique," *Cryogenics*, vol. 16, no. 4, pp. 217–219, Apr. 1976.

[24] K. Kobayashi *et al*., "Development of a superconducting joint resistance evaluation system," *IEEE Trans. Appl. Supercond.*, vol. 30, no. 4, Jun. 2020, Art. no. 9000204.

[25] R. H. Koch, V. Foglietti, W. J. Gallagher, G. Koren, A. Gupta, and M. P. A. Fisher, "Experimental evidence for vortex-glass superconductivity in Y-Ba-Cu-O," *Phys. Rev. Lett.*, vol. 63, no. 14, pp. 1511–1514, Oct. 1989.

[26] S. Awaji, R. Ishihara, K. Watanabe, K. Shikimachi, N. Hirano, and S. Nagaya, "Anisotropy of the Critical Current Density and Intrinsic Pinning Behaviors of $YBa_2Cu_3O_y$ Coated Conductors," *Appl. Phys. Express*, vol. 4, no. 1, Jan. 2011, Art. no. 013101.

[27] G. Nishijima, H. Kitaguchi, S. Awaji, and H. S. Shin, "Transport property measurement of practical coated conductor with copper stabilizer," *AIP Conf. Proc.*, vol. 1435, pp. 258–264, Jun. 2012.

[28] G. Nishijima, Y. Tsuchiya, H. Kitaguchi, T. Nishimura, and T. Kato, "I_c–B–T Evaluation for High-T_c Superconductors in Pressurized/Depressurized Liquid Nitrogen," *IEEE Trans. Appl. Supercond.*, vol. 23, no. 2, Jun. 2013, Art. no. 8000703.

[29] K. Yamafuji and T. Kiss, "Current–voltage characteristics near the glass–liquid transition in high-T_c superconductors," *Physica C*, vol. 290, no. 1–2, pp. 9–22, Oct. 1997.

[30] M. Inoue *et al*., "Estimation of E–J characteristics in a YBCO coated conductor at low temperature and very high magnetic field," *Physica C*, vol. 392–396, no. 2, pp. 1078–1082, Oct. 2003.

[31] Y. Onodera *et al*., "Critical current density in $Gd_1Ba_2Cu_3O_{7-\delta}$ coated conductor under the influence of flux creep," *Phys. Proc.*, vol. 67, pp. 926–930, Jul. 2015.

[32] Y. Takeda, G. Nishijima, K. Inoue, Y. Takano, and H. Kitaguchi, "The effect of intermediate layer densification on the critical current of a Bi-2223 superconducting joint," *Supercond. Sci. Technol.*, vol. 36, no. 3, Jan. 2023, Art. no. 035004.

[33] T. Kato *et al*., "Nanostructural evolution of intermediate grown superconducting joint layers between $GdBa_2Cu_3O_y$ coated conductors," *Supercond. Sci. Technol.*, vol. 33, no. 10, Aug. 2020, Art. no. 105008.

[34] Z. Wu, K. Higashikawa, and T. Kiss, "Continuous Measurement on Electric-Field Versus Current-Density Characteristics of REBCO Coated Conductors in the Electric-Field Window From 10−2 Down to 10−11 V/m," *IEEE Trans. Appl. Supercond.*, vol. 33, no. 5, Aug. 2023, Art. no. 6601705.

[35] C. Lucas, P. Cayado, H. Rijckaert, K. Konstantopoulou, D. Nardelli, and C. Senatore, "Critical current degradation of commercial REBCO coated conductors under thermomechanical loads," *Supercond. Sci. Technol.*, vol. 37, no. 12, Nov. 2024, Art. no. 125014.